

Comparison of different mass transfer models for direct contact membrane distillation flux evaluation

Khadije El Kadi^{a,b}, Konstantinos Moustakas^c, Isam Janajreh^{a,b,*}

^aCenter for Membrane and Advanced Water Technology, Khalifa University of Science and Technology, Abu Dhabi, United Arab Emirates, emails: isam.janajreh@ku.ac.ae (I. Janajreh), khadije.elkadi@ku.ac.ae/khadijeelkadi@gmail.com (K. El Kadi)

^bMechanical Engineering Department, Masdar Institute, Khalifa University of Science and Technology, Abu Dhabi, United Arab Emirates

^cUnit of Environmental Science and Technology, National Technical University of Athens, Athens, Greece, email: konmoust@central.ntua.gr (K. Moustakas)

Received 24 October 2019; Accepted 26 February 2020

ABSTRACT

The discrepancies between mass flux prediction models is a major issue in membrane distillation (MD) literature. Computational fluid dynamics model was used to capture the driving pressure gradient across the membrane using a range of inlet feed temperatures and flow velocities. Hence, a comparison between the most pronounced prediction models is presented. Validation and error estimation of those models is done using recent literature experimental work. Results revealed that all current models follow and reserve the same trend of actual mass flux. Nevertheless, actual mass flux merges to a higher estimated model when flow velocity increased, which as a result decreased the error estimate of that model from 0.90 at low flow velocity to 0.03 at high flow velocity. Results also show the inapplicability of some models as the dusty gas model and Multi-pore size model in MD, while the precision of the others. This work also eliminates the doubts of Poiseuille flow as it clearly showed its significance in mass flux prediction. Current models are acceptable for the time being the stage of MD and are useful tools for sensitivity studies.

Keywords: Membrane distillation; Kinetic theory of gases; Knudsen diffusion; Molecular diffusion; Viscous flow; Mass flux

1. Introduction

The working principle of membrane distillation (MD) relies on the non-isothermal condition across the membrane which creates a driving pressure gradient allowing mass transport from one side of a membrane to another. This technology has been widely studied in all aspects [1–9]. The transport of water vapor through the membrane pores in an MD process follows Kinetic Theory of Gases and is governed by three main contributors: (i) Knudsen diffusion, (ii) Poiseuille flow, and (iii) molecular diffusion [10,11]. Based on process conditions and membrane structure (mainly pore size and mean free path), one of those

contributors dominates water vapor transport [11]. If the membrane pore size is relatively larger than the mean free path of water vapor molecules, the molecule-molecule collisions are dominant among the molecule-pore wall ones and vapor transport takes place through a viscous (or Poiseuille) flow. Theoretically, viscous flow is absent in most of MD configurations where total pressure is fixed at 1 atm due to the presence of air molecules inside the pores [12]. Exceptionally, Poiseuille flow occurs when operation under vacuum, for example, vacuum membrane distillation, where air molecules are eliminated from membrane pores allowing a change in total pressure across the membrane [13,14]. On the other hand, if the mean free path is large enough

* Corresponding author.

compared to the pore size, then the molecule-pore wall collisions are dominant over the molecule–molecule ones and therefore, vapor transport takes place via Knudsen diffusion flow. Else, molecular diffusion takes place when stagnant air is trapped within membrane pores. Table 1 provides a brief summary of the three different routes of mass transport along with their mathematical formulations.

In fact, due to the non-uniformity of membrane pores sizes, more than one mechanism may occur simultaneously. As a result, several combination models have been attempted in the literature to predict – in a better agreement – the actual membrane permeability [10,13–18]. Dusty gas model (DGM) is the most general model for predicting flux through porous media which was firstly described by Maxwell in 1860 [13,19]. DGM combines the three different models, that is, Knudsen, Poiseuille, and molecular flows, and is arranged as seen in the electrical analogy circuit represented in Table 2. Although the DGM was originally proposed for isothermal systems, it was applied to MD by neglecting the surface diffusion term and adding thermal terms that assume average temperature across the membrane [13,20,21]. Although some recent studies showed the inapplicability of DGM as it does not emphasize the exact effect of temperature, people are still using it to describe mass transfer in MD [16,22,23]. A combined diffusion mass transfer coefficient (Table 2) for MD membranes with intermediate pore sizes has been also proposed and tested where resistances of both molecular and Knudsen diffusions occur at the same time [11,15,24]. This model showed better conversion to experimental mass flux when compared to the individual effect of both Knudsen diffusion and molecular diffusion [22]. Researchers had a great interest in this model precisely for flux prediction of direct contact membrane distillation (DCMD) configuration that operates at atmospheric pressure and thus lacks the condition of viscous flow [25,26]. Instead, Schofield et al. [14] proposed and studied a combined empirical model where mass transport occurs in the Knudsen/Poiseuille transition region. The model showed excellent agreement with experimental results for deaerated membranes [14]. The model was further modified by adding molecular

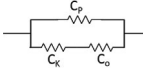
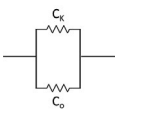
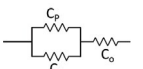
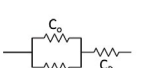
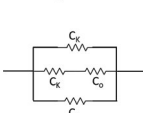
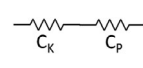
diffusion resistance to account for conditions where the partial pressure of air is substantial (Table 2) [27]. More recent study by Ding et al. [16] proposed a three-parametric model that includes molecular/Knudsen transition diffusion and Poiseuille flow to predict the water vapor flux for MD. The model appreciated and validated the contribution of Poiseuille flow in flux prediction contrasting the combined diffusion model that was discussed earlier. Damtie et al. [28] found an excellent agreement of Ding's model with their results when a range of polyvinylidene difluoride membranes were tested in DCMD configuration. Unlike the above models, Phattaranawik et al. [17] have derived a mass transfer model for DCMD that includes the effect of pore size distribution using multiple combinations of Knudsen and molecular diffusions and their transitions as seen in the electrical analog in Table 2. Findings were similar to Schofield et al. [15] where the transition region between Knudsen and molecular diffusion dominates mass transport [17]. Chen et al. [18] attempted to describe the overall membrane mass transport coefficient using the addition of Knudsen and Poiseuille permeabilities. This approach was firstly proposed in 1954 for flow along capillary tubes [14]. Although this combined model showed reasonable success, however, it was limited in literature due to its complicated requirement of several membrane morphology parameters [14]. A comprehensive summary of the discussed models along with their corresponding electrical analog and overall membrane coefficient is tabulated in Table 2.

Those models are the most pronounced throughout the history of MD in attempts to accurate prediction of mass flux. Nevertheless, a lack of understanding of the conditions of when one model is more favorable than the others is present. To the best of the authors knowledge, nobody has done a comparison of those models in a single study. This work acts as a validation of six different mass transport models in a flat-sheet DCMD module using both experimental and numerical assessments. Further, error estimation will be performed on the predicted mass fluxes. The aim of this study is to establish a reference prediction model that offers a reliable sound to be employed in estimating a wide range of MD membranes mass fluxes.

Table 1
Main transport mechanism of mass transfer in porous media [10–11]

Mass transport	Mathematical formula	When to consider?
Knudsen diffusion	$C_k = 1.064 \frac{\epsilon r}{\tau \delta} \left(\frac{M_w}{RT} \right)^{\frac{1}{2}}$	<ul style="list-style-type: none"> • When molecule-pore wall collisions are dominant over the molecule–molecule collisions (mean free path is large in relative with pore size)
Molecular (ordinary) diffusion	$C_0 = \frac{M_w \epsilon PD}{RT \delta P_a \tau}$ $PD = 1.89510^{-5} T^{2.072}$	<ul style="list-style-type: none"> • Presence of stagnant air molecules
Poiseuille (viscous) flow	$C_p = 0.125 \frac{\epsilon r^2}{\tau \delta} \frac{M_w P_m}{\mu RT}$	<ul style="list-style-type: none"> • Variable total pressure across the membrane (not the case of DCMD) • Large pore size

Table 2
Most pronounced combination models predicting MD membrane mass transfer coefficient

Combined model name	Electrical analogue	Membrane mass transfer coefficient
1. Dusty gas model [13]		$C_m = \left(\frac{1}{C_p} + \frac{1}{C_k + C_o} \right)^{-1}$
2. Combined diffusion model [15]		$C_m = \left(\frac{1}{C_o} + \frac{1}{C_k} \right)^{-1}$
3. Schofield's model [14]		$C_m = \left(\frac{1}{C_k} + \frac{1}{C_p} \right)^{-1} + C_o$
4. Ding et al. model [16]		$C_m = \left(\frac{1}{C_k} + \frac{1}{C_o} \right)^{-1} + C_p$
5. Multi-pore size model [17]		$C_m = \left(\frac{1}{C_o} + \frac{1}{C_k} + \frac{1}{C_k + C_o} \right)^{-1}$
6. Chen et al. model [18]		$C_m = C_k + C_p$

2. Methodology

The scope of this work is first to evaluate numerically mass flux of DCMD using a computational fluid dynamics (CFD) model that will be coupled with the different membrane transport models as discussed earlier in Table 2. Due to the discrepancy of these models, experimental assessment is necessary to be conducted. As such, the theoretically evaluated mass fluxes from different models are validated experimentally from a recent literature work of the author's colleagues [29]. The referenced experimental setup will be briefly described. Lastly, error estimation and correction are established for mass flux results from the different models taking the experimental results as a baseline.

2.1. Numerical model setup

A non-isothermal three-dimensional (3-D) CFD model of flat sheet DCMD process is developed. Dimensions of the DCMD module are selected to be identical to the experiment setup of Castillo et al. [29]. In their study, the experimental module length, width, and channel depth were 8.10 cm × 5.10 cm × 0.23 cm, respectively, while a commercial polytetrafluoroethylene (PTFE) flat sheet membrane with a mean pore size of 0.22 μm, average porosity of 75%, and membrane thickness of 179 μm, was used. Additionally, counterflow with fresh deionized water as permeate and brine at 3.5% salinity have been used with flow velocity ranges between 0.08 to 0.18 m/s and various temperature values in both feed and permeate channels [29]. They have used several spacers configurations, however in this work,

the baseline module results are considered. A schematic diagram of the simulated system setup is illustrated in Fig. 1.

Eventually, the 3-D geometry is discretized as shown in Fig. 2 using a structural volume mesh type with a reasonable resolution to enable capturing boundary layers. Consisting of three zones, the mesh is perfectly orthogonal with the maximum cell volume of 2.23E-13 m³ and maximum face area of 5.14E-07 m² resulting in 3,686,400 computational cells as a baseline. Additionally, four levels of meshing were established covering two refined and two coarse in the quest of reaching to this baseline discretized mesh domain and in the assessment of the solution mesh dependency.

The system is governed by the conjugated steady incompressible Navier–Stocks and energy equations as follows:

$$\nabla \cdot (\rho \vec{v}) = 0 \tag{1}$$

$$\nabla \cdot (\rho \vec{v} \vec{v}) = -\nabla P + \mu \nabla^2 \vec{v} + \rho \vec{g} \tag{2}$$

$$\nabla \cdot (\rho \vec{v} H) = \nabla \cdot (k \nabla T) \tag{3}$$

Channel inlet boundary conditions follow the Dirichlet conditions (prescribed velocity and temperature), while outlets are set to Neumann boundary conditions (zero velocity gradient and constant atmospheric pressure). Bulk and side walls are insulated thermally, that is, Neumann boundary condition, and subjected to no-slip condition while the top and bottom membrane surfaces were thermally coupled with the feed and permeate channel. As the PTFE membrane was used in the experimental study of Castillo et al. [29], the thermal properties of PTFE were set in the numerical model to include its effect on the driving temperature and pressure. A range of feed temperatures and inlet velocities were chosen to be identical to the setup done by Castillo et al. [29] and is summarized in Table 3. Meanwhile, inlet permeates temperature were fixed for all runs at 22°C.

Solutions were carried out using a fluent commercial CFD code that is based on the finite volume approach and segregated solver [30,31]. Pressure and velocity were coupled together using SIMPLE algorithm, that is, the semi-implicit method for pressure-linked equations, with the second-order upwind spatial scheme. Very tight convergence residuals are set for continuity (1E-15) and momentum and energy (1E-6) equations. Mesh dependency study is done on the basis of the attained temperature profile and its error estimate based on the refined mesh. The profile of the temperature at the mid-span is used while running at 0.13 m/s flow velocity and temperatures of 55°C and 22°C for the hot and cold channel, respectively. The relative error is computed based on the values obtained from the refined mesh II level as given in Eq. (4):

$$T_{Rel.Erro} = \frac{1}{n} \sum_{i=1}^n \frac{\sqrt{T_{fine}^i - T_{current}^i}^2}{T_{fine}^i} \times 100 \tag{4}$$

The subscripts fine and current indicates the very refined/fine mesh and current mesh, respectively. The baseline mesh results in near 0.5% error which also within reasonable

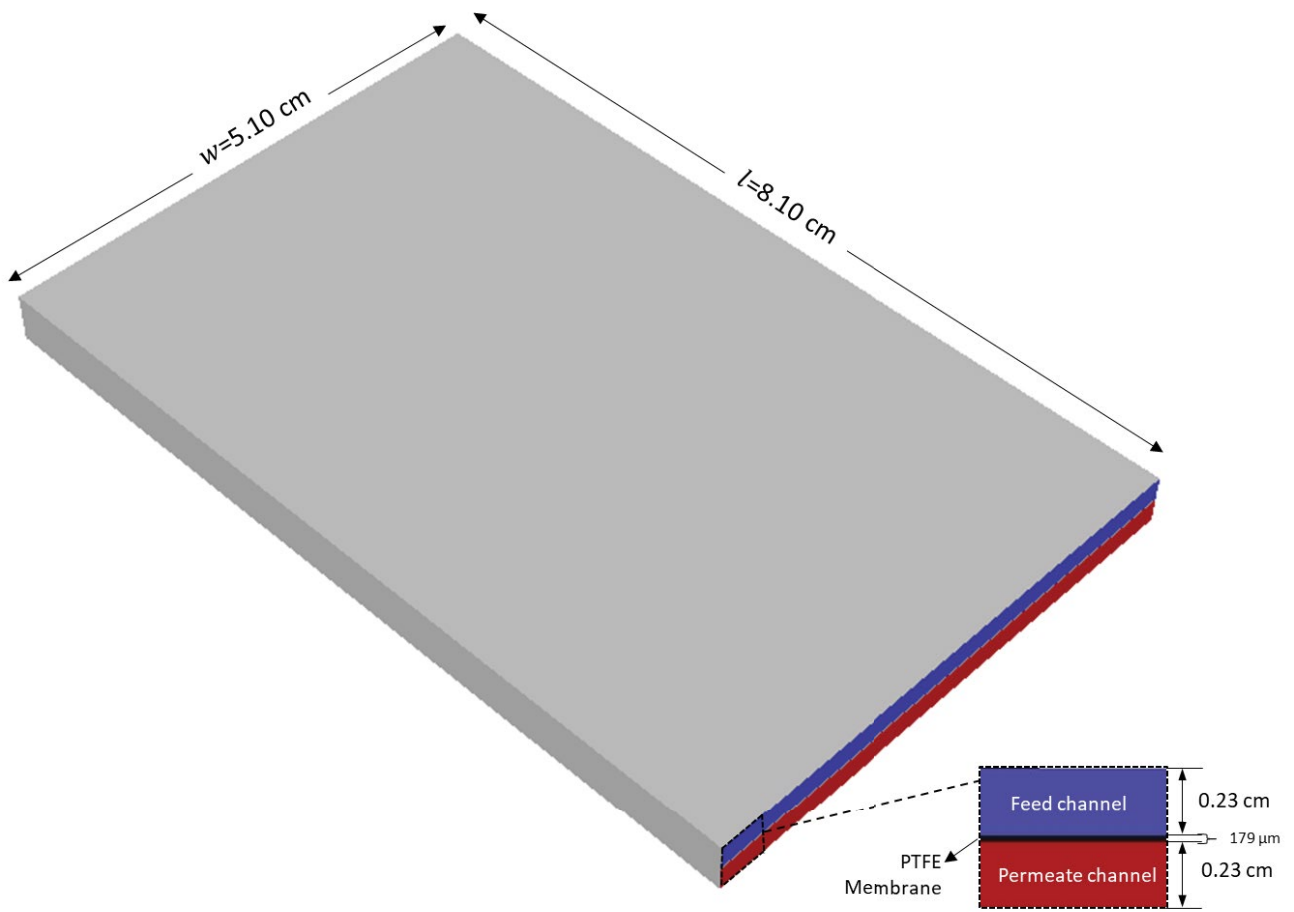


Fig. 1. Schematic diagram of DCMD experimental module geometry of Castillo et al. [29].

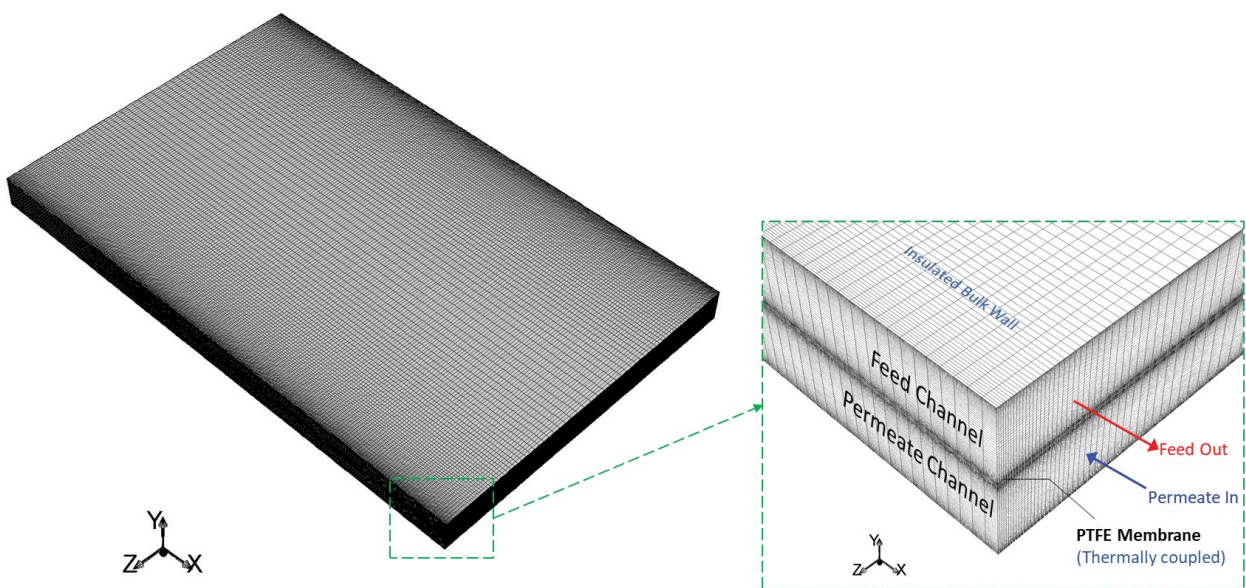


Fig. 2. 3-D mesh of DCMD module and boundary conditions setup.

deviation from the refined level I mesh (i.e., RE = 0.45%) while is deviating nearly 1.2% and 2.2% from the coarse I and II levels, respectively. It should be noted that the size of the refined meshes files exceeds 0.5GB which requires special graphic cards for post-processing.

2.2. Mass flux assessment

The general expression of permeated mass flux in an MD process is formulated as the following:

$$J = C_m (P_f^{sat} - P_p^{sat}) \tag{5}$$

The gradient of transmembrane saturated pressure occurs due to the temperature polarization at the top and bottom membrane surfaces. A variable and important parameter called temperature polarization coefficient (TPC) is presented to quantify this phenomenon. It represents the ration of the channels cross membrane temperature difference to that of the bulk and is expressed in Eq. (6) as:

$$TPC = \frac{T_{m,f} - T_{m,p}}{T_{b,f} - T_{b,p}} \tag{6}$$

Generally, from membrane surface temperatures, the Antoine equation is used to estimate the saturation pressure of water at both the feed and permeate sides:

$$P_i^{sat} = \exp \left(23.1964 - \left(\frac{3,816.44}{T_{m,i} - 46.13} \right) \right), i \in \{f, p\} \tag{7}$$

As discussed earlier, the membrane mass transfer coefficient, C_m , is theoretically estimated using the different combination models presented in Table 2. Castillo

et al. [29] baseline study evaluated the DCMD experimental permeated mass flux across the active membrane area under the operation conditions stated earlier using an electronic balance. Results of experimental mass flux were reported as permeate volume per active area of a square meter per hour (L/m²/h) and are presented in Table 4.

2.3. Validation and error estimation assessment

The ultimate goal of this study is to validate prediction models of the mass transport through MD membranes and finally targeting a reference model that can be used in a wide range of sensitivity studies. Mass flux results from the experimental setup is used as the reference of validation. In order to quantify the difference, error between experimentally investigated mass flux and numerically investigated mass fluxes is evaluated for each combined model (i) stated in Table 2 through the following equation:

$$E = \frac{\sqrt{(J_i - J_e)^2}}{J_e}, i \in \{1, 2, 3, 4, 5, 6\} \tag{8}$$

3. Results and discussion

The CFD model was used to run 15 cases having different inlet velocity and feed temperature as were presented in Table 3. Fig. 3 shows velocity vectors of the three ranges of inlet velocities presenting clearly the fully developed flow through DCMD channels. It should be noted that the figure is taken at a middle x–y cross-sectional plane. A change in temperature distribution and polarization at membrane surfaces owed by the increase of inlet velocity are also observed. As a result, average TPC increases from 0.59, 0.63 to 0.65 for inlet velocity of 0.08, 0.13, and 0.18 m/s, respectively. Additionally, different feed inlet temperature has been

Table 3
Channels inlet velocity and feed intel temperatures for different runs, permeate temperature was kept at fixed value of 22°C

Run	Channels inlet velocity (m/s)	Feed inlet temperature (°C)
V1T1	0.08	45
V1T2		50
V1T3		55
V1T4		60
V1T5		65
V2T1	0.13	45
V2T2		50
V2T3		55
V2T4		60
V2T5		65
V3T1	0.18	45
V3T2		50
V3T3		55
V3T4		60
V3T5		65

Table 4
Experimental mass flux data retrieved from [29]

Run	Experimental mass flux (L/m ² h)
V1T1	7.68
V1T2	9.30
V1T3	12.67
V1T4	17.58
V1T5	24.26
V2T1	12.42
V2T2	14.76
V2T3	19.6
V2T4	26.4
V2T5	35.81
V3T1	15.42
V3T2	20.64
V3T3	28.48
V3T4	38.95
V3T5	52.04

set alternatively for each inlet velocity, resulting in 15 different cases. Fig. 4 depicts temperature distribution across the DCMD model for different inlet feed temperatures while flow velocity was fixed at a moderate speed of 0.13 m/s in both channels.

Results of average mass flux from the six different mass transport prediction models and the experimentally investigated mass flux through a range of feed temperatures and flow velocity of 0.08, 0.13, and 0.18 m/s are presented in Figs. 5–7, respectively. It is clearly noticed that the trend is reserved and captured in all models. Nevertheless, experimental mass flux data merge to a higher estimated model when the flow velocity is increased. At low flow

velocity, that is, 0.08 m/s, experimental data intermediates between Schofield’s model [14], that is, M3, and Ding et al. [16] model, that is, M4. At moderate flow velocity, however, the experimental mass flux curve is almost approaching the Schofield’s model [14], that is, M3. Increasing the inlet flow velocity to 0.18 m/s, the experimental mass flux data have shifted up to perfectly merge with Chen et al. model [18], that is, M6.

Relative errors of the six prediction models were evaluated as per Eq. (8) and depicted in Fig. 8 by taking the average value of each model at a certain flow velocity. Results show obviously the inapplicability of the DGM, that is, M1, in DCMD technology with the maximum error ratio among

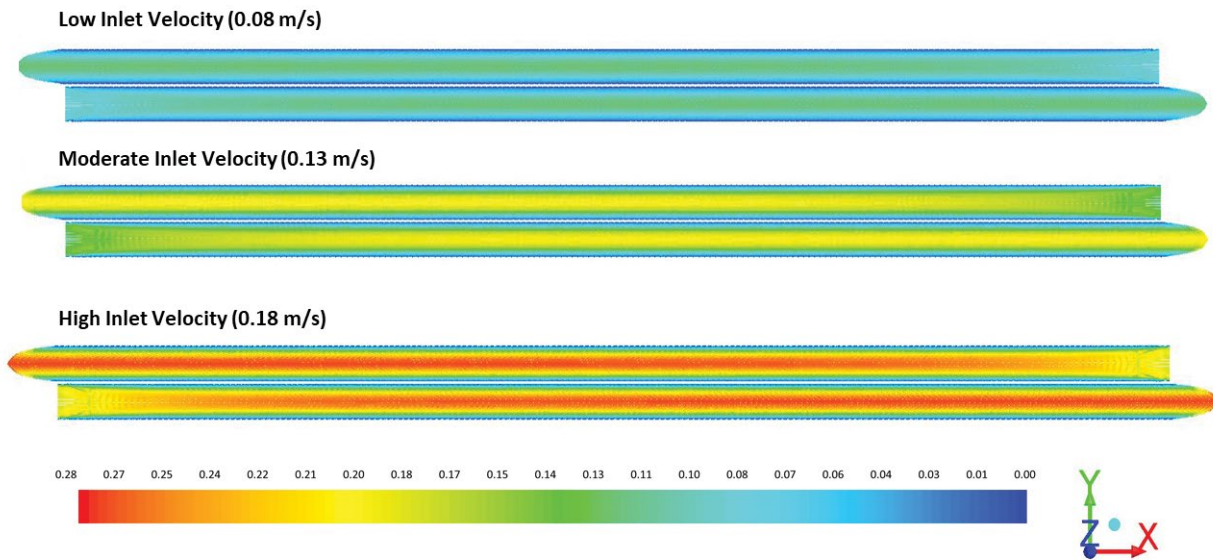


Fig. 3. Velocity vectors in a mid-plane (x - y) of 3-D DCMD model running at three ranges of inlet velocities.

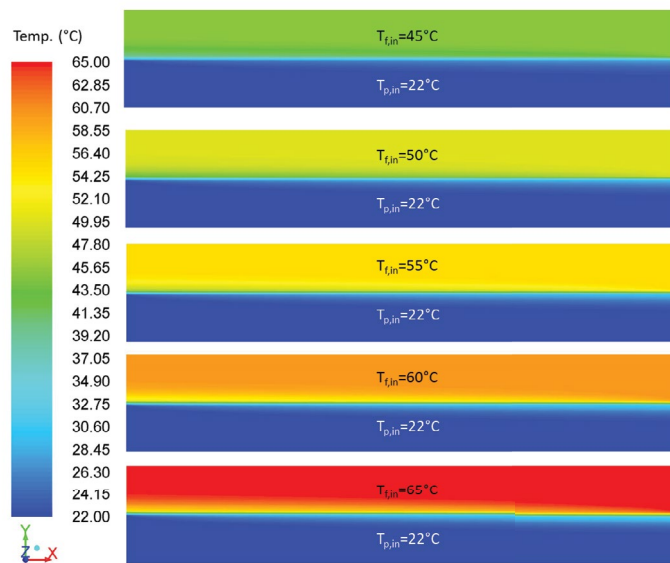


Fig. 4. Contours of temperature at a mid-plane (x - y) of the DCMD 3-D model operating at a range of inlet feed temperature 45°C–65°C (scaled $\times 3$ in y -axis direction for better picturing).

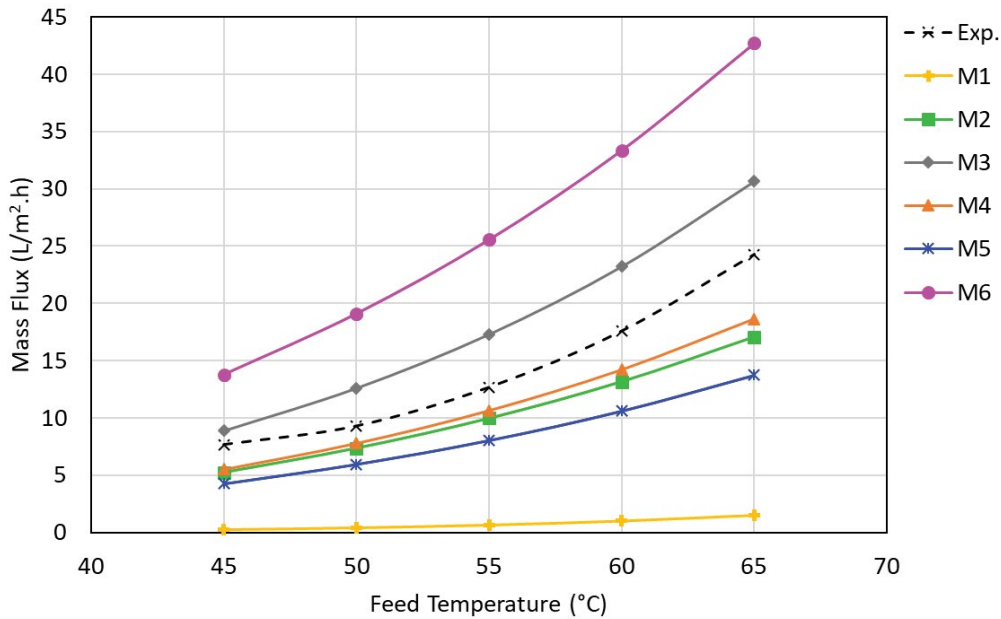


Fig. 5. Average mass flux of DCMD evaluated using different mass transport models and experimental study at low flow velocity of 0.08 m/s.

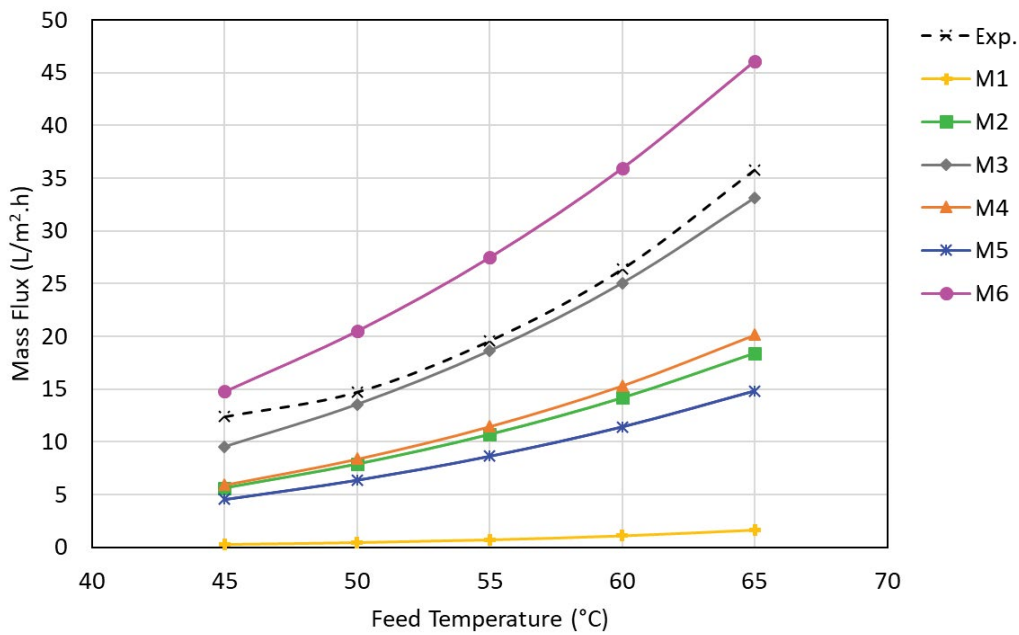


Fig. 6. Average mass flux of DCMD evaluated using different mass transport models and experimental study at moderate flow velocity of 0.13 m/s.

other models ($E > 0.9$ in all velocity ranges). This is explained by the iso-thermal assumption of the model which as a result did not reflect the thermal effect across membrane surfaces. The multi-pore size model, that is, M5, have also a very low prediction of mass flux where the error fraction varied between 0.40 and 0.69. By comparing M5 results with M2, that is, combined diffusion model, one can notice a

better agreement of the latter than the earlier. These findings match with literature as the molecular/Knudsen transition dominates the transport in higher rates than individual transport of both diffusions [15,17]. When the Poiseuille flow term was added in series with the transition diffusion term in Ding et al. model [16], that is, M4, the model exhibited better agreement with experimental data. This is another

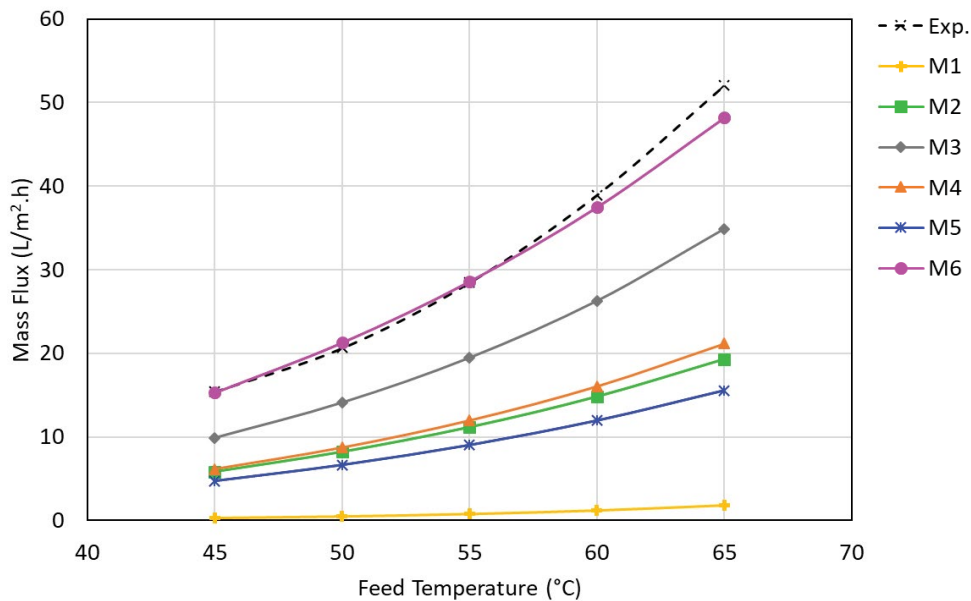


Fig. 7. Average mass flux of DCMD evaluated using different mass transport models and experimental study at high flow velocity of 0.18 m/s.

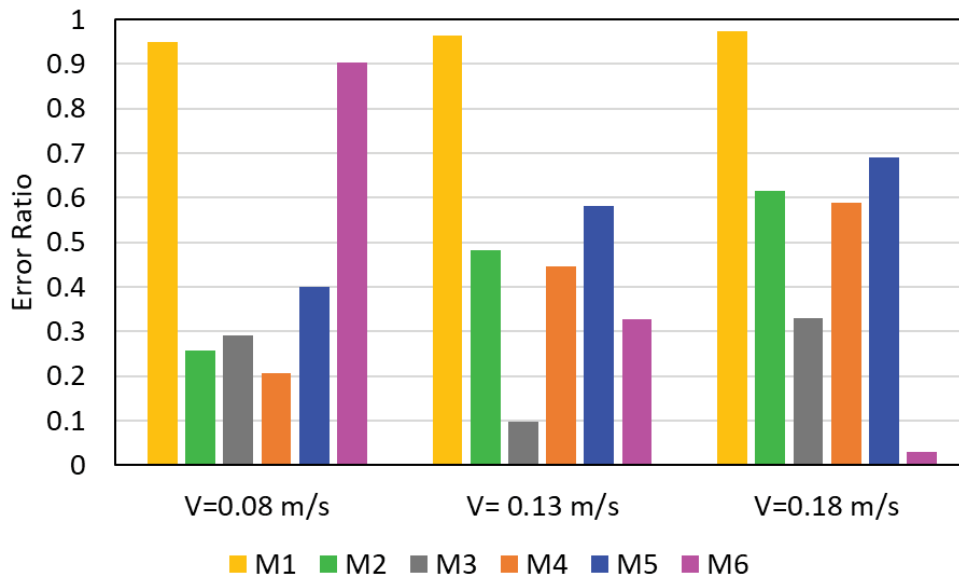


Fig. 8. Error estimation of different mass prediction models compared to the experimentally evaluated mass flux.

good indication that Poiseuille flow plays an important role in mass transport through DCMD membranes. On the other hand, Schofield’s model [14], M3, approaches the experimental mass flux with the least error of 0.09 when operating at moderate flow velocity, that is, 0.13 m/s. In this model, the Poiseuille/Knudsen transition takes place simultaneously with molecular diffusion. Finally, Chen et al. model [18], that is, M6, which consists of both Knudsen and Poiseuille transports in series configuration represents a unique trend in each flow velocities. As seen in the mass flux plots, this model is always presenting the highest prediction over a

range of flow velocity. However, as the experimental mass flux behaves differently in each flow velocity range, M6 recorded its highest error of 0.90 at low velocity and its lowest error of 0.03 at the high-velocity range. This indicates the importance of the molecular diffusion role when operating at low velocities. In contrast, it also provides good evidence that Poiseuille flow owns a significant effect on mass transport across MD membranes, along with Knudsen diffusion.

Within the current operating range of most of MD tests in literature, M3, M4, M6, and M2 are acceptable prediction models with reserved trends if they are employed at their

optimum range of flow velocity. Though, if the operational range of MD is expanded in the future, this work might need to be repeated.

4. Conclusion

Comprehensive work has been done on the validation of the different mass flux prediction models available in the literature. With the aid of CFD and an earlier experimental study, the performance of DCMD along with error estimation was evaluated for the different prediction models. Those prediction models were basically a combination of three models: the Knudsen diffusion model, the molecular diffusion model, and the Poiseuille viscous flow model. Results revealed that the prediction models accuracy are highly dependent on the channels flow velocity range. All models except the dusty gas were very responsive and well behaved when the feed temperature is varied. At the low flow velocity range, Ding's model that is largely affected by the molecular diffusion model showed the least error. For medium and high-velocity ranges, however, the Schofield's and Chen's models at which the Poiseuille flow is dominant, showed, respectively, the least errors. This study established the level of deviation that one may encounter in the usage of each prediction model. It also opens further research opportunities in integrating correction factors or re-weighting model parameters to emerge these predictions. Finally, as MD is getting into large scale commercial implementation and deployment, providing a reliable estimation of the desalinated flux and under a wide range of operating conditions is indispensable.

Acknowledgments

This publication is based upon work partially supported by the Khalifa University under Award Nos. X20116-000022 and RC2-2018-009. The Center for Membrane and Advanced Water Technology at Khalifa University is also acknowledged.

Symbols

C	—	Mass transfer coefficient, $\text{kg}/(\text{m}^2 \text{ Pa s})$
ε	—	Porosity factor, —
r	—	Pore radius, m
τ	—	Tortuosity factor, —
δ	—	Membrane thickness, m
M	—	Molecular weight, kg/mol
R	—	Universal gas constant, $\text{J}/(\text{mol K})$
T	—	Temperature, K
P	—	Pressure, Pa
D	—	Water diffusion coefficient, m^2/s
μ	—	Dynamic viscosity, $\text{kg}/(\text{m s})$
t	—	Time, s
ρ	—	Density, kg/m^3
\bar{v}	—	Flow velocity, m/s
\bar{g}	—	Gravitational acceleration, m/s^2
H	—	Overall sensible enthalpy, kJ/kg
J	—	Permeation mass flux, $\text{L}/(\text{m}^2 \text{ h})$
n	—	Number of datapoint

Superscripts

sat — Saturation

Subscripts

m	—	Membrane
K	—	Knudsen model
P	—	Poiseuille model
O	—	Molecular model
w	—	Water
a	—	Air
f	—	Feed
p	—	Permeate
b	—	Bulk
e	—	Experimental

References

- [1] M. Albeirutty, N. Turkmen, S. Al-Sharif, S. Bouguecha, A. Malik, O. Faruki, An experimental study for the characterization of fluid dynamics and heat transport within the spacer-filled channels of membrane distillation modules, *Desalination*, 430 (2018) 136–146.
- [2] Y. Taameh, K. Bataineh, Improving the performance of direct contact membrane distillation utilizing spacer-filled channel, *Desalination*, 408 (2017) 25–35.
- [3] H. Chang, J.-A. Hsu, C.-L. Chang, C.-D. Ho, T.-W. Cheng, Simulation study of transfer characteristics for spacer-filled membrane distillation desalination modules, *Appl. Energy*, 185 (2017) 2045–2057.
- [4] K.E. Kadi, R. Hashaikh, R. Ahmed, I. Janajreh, Design and performance evaluation of a portable hybrid desalination unit using direct contact membrane distillation in dual configuration, *Energy Procedia*, 158 (2019) 904–910.
- [5] I. Janajreh, K. El Kadi, R. Hashaikh, R. Ahmed, Numerical investigation of air gap membrane distillation (AGMD): seeking optimal performance, *Desalination*, 424 (2017) 122–130.
- [6] A. Khalifa, H. Ahmad, M. Antar, T. Laoui, M. Khayet, Experimental and theoretical investigations on water desalination using direct contact membrane distillation, *Desalination*, 404 (2017) 22–34.
- [7] K.E. Kadi, I. Janajreh, R. Hashaikh, Low Energy Desalination via DCMD: The Role of Superhydrophobicity and Optimal Flow Conditions, In: 2017 International Renewable and Sustainable Energy Conference (IRSEC), 2017, pp. 1–6.
- [8] H. Yu, X. Yang, R. Wang, A.G. Fane, Analysis of heat and mass transfer by CFD for performance enhancement in direct contact membrane distillation, *J. Membr. Sci.*, 405–406 (2012) 38–47.
- [9] M. Khayet, T. Matsuura, Membranes Used in MD and Design, In: *Membrane Distillation Principles and Application*, Elsevier, Amsterdam, 2011, pp. 17–40.
- [10] M. Khayet, A. Velázquez, J.I. Mengual, Modelling mass transport through a porous partition: effect of pore size distribution, *J. Non-Equilib. Thermodyn.*, 29 (2004) 279–299.
- [11] M. Khayet, M. Godino, J. Mengual, Modelling transport mechanism through a porous partition, *J. Non-Equilib. Thermodyn.*, 26 (2001) 1–14.
- [12] J. Phattaranawik, R. Jiratananon, A.G. Fane, C. Halim, Mass flux enhancement using spacer filled channels in direct contact membrane distillation, *J. Membr. Sci.*, 187 (2001) 193–201.
- [13] K.W. Lawson, D.R. Lloyd, Review: membrane distillation, *J. Membr. Sci.*, 124 (1997) 1–25.
- [14] R.W. Schofield, A.G. Fane, C.J.D. Fell, Gas and vapour transport through microporous membranes. I. Knudsen-Poiseuille transition, *J. Membr. Sci.*, 53 (1990) 159–171.
- [15] R. Schofield, A. Fane, C. Fell, Heat and mass transfer in membrane distillation, *J. Membr. Sci.*, 33 (1987) 299–313.

- [16] Z. Ding, R. Ma, A.G. Fane, A new model for mass transfer in direct contact membrane distillation, *Desalination*, 151 (2003) 217–227.
- [17] J. Phattaranawik, R. Jiratananon, A.G. Fane, Effect of pore size distribution and air flux on mass transport in direct contact membrane distillation, *J. Membr. Sci.*, 215 (2003) 75–85.
- [18] T.-C. Chen, C.-D. Ho, H.-M. Yeh, Theoretical modeling and experimental analysis of direct contact membrane distillation, *J. Membr. Sci.*, 330 (2009) 279–287.
- [19] J.C. Maxwell, V. Illustrations of the dynamical theory of gases. — Part I. On the motions and collisions of perfectly elastic spheres, *London Edinburgh Dublin Philos. Mag. J. Sci.*, 19 (1860) 19–32.
- [20] M. Khayet, T. Matsuura, Chapter 10: Direct Contact Membrane Distillation, M.K. Matsuura, Ed., *Membrane Distillation*, Elsevier, Amsterdam, 2011, pp. 249–293.
- [21] L. Martínez, F. J. Florido-Díaz, Theoretical and experimental studies on desalination using membrane distillation, *Desalination*, 139 (2001) 373–379.
- [22] Ó. Andriessdóttir, C.L. Ong, M. Nabavi, S. Paredes, A.S.G. Khalil, B. Michel, D. Poulikakos, An experimentally optimized model for heat and mass transfer in direct contact membrane distillation, *Int. J. Heat Mass Transfer*, 66 (2013) 855–867.
- [23] M.M.A. Shirazi, A. Kargari, A.F. Ismail, T. Matsuura, Computational fluid dynamic (CFD) opportunities applied to the membrane distillation process: state-of-the-art and perspectives, *Desalination*, 377 (2016) 73–90.
- [24] M. Qtaishat, T. Matsuura, B. Kruczek, M. Khayet, Heat and mass transfer analysis in direct contact membrane distillation, *Desalination*, 219 (2008) 272–292.
- [25] M. Khayet, Membranes and theoretical modeling of membrane distillation: a review, *Adv. Colloid Interface Sci.*, 164 (2011) 56–88.
- [26] J. Zhang, S. Gray, J.-D. Li, Modelling heat and mass transfers in DCMD using compressible membranes, *J. Membr. Sci.*, 387–388 (2012) 7–16.
- [27] R. Schofield, A. Fane, C. Fell, Gas and vapour transport through microporous membranes. II. Membrane distillation, *J. Membr. Sci.*, 53 (1990) 173–185.
- [28] M.M. Damtie, Y.C. Woo, B. Kim, K.-D. Park, R.H. Hailemariam, H.K. Shon, J.-S. Choi, Analysis of mass transfer behavior in membrane distillation: mathematical modeling under various conditions, *Chemosphere*, 236 (2019) 124–289.
- [29] E.H.C. Castillo, N. Thomas, O. Al-Ketan, R. Rowshan, R.K. Abu Al-Rub, L.D. Nghiem, S. Vigneswaran, H.a. Arafat, G. Naidu, 3D printed spacers for organic fouling mitigation in membrane distillation, *J. Membr. Sci.*, 581 (2019) 331–343.
- [30] K. El Kadi, I. Janajreh, R. Hashaikeh, R. Ahmed, Refinery processed water treatment via the low energy direct contact membrane distillation (DCMD), *Oil Gas Sci. Technol.*, 74 (2019).
- [31] ANSYS Fluent, Release 12.0, Help System, Theory Guide: ANSYS Inc., 2009.